ACS Medicinal Chemistry Letters

LETTER

pubs.acs.org/acsmedchemlett

Hydrophobic Binding Hot Spots of Bcl-xL Protein−Protein Interfaces by Cosolvent Molecular Dynamics Simulation

Chao-Yie Yang and Shaomeng Wang*

Comprehensive Cancer Center, Departments of Internal Medicine, Pharmacology, and Medicinal Chemistry, University of Michigan, 1500 East Medical Center Drive, Ann Arbor, Michigan 48109-0934, United States

Supporting Information

ABSTRACT: Identifying binding hot spots in protein−protein interfaces is important for understanding the binding specificity and for the design of nonpeptide, small molecule inhibitors. Molecular dynamics simulation in the isopropanol/water cosolvent environment and in water was employed to investigate Bcl-xL protein, which has a highly flexible, large, and primarily hydrophobic binding site. Simulations of either the apo- or holocrystal structures of the Bcl-xL in pure water fail to generate conformations found in the cocrystal structures of Bcl-xL in complex with its binding partners due to hydrophobic collapse. In contrast, simulations in cosolvent starting either from the apo- or holocrystal structure of the Bcl-xL yield binding-site conformations similar to that found in the cocrystal structures of Bcl-xL. Hydrophobic binding hot spots identified using the conformations from the cosolvent simulations are in excellent agreement with experimental structural data of known inhibitors. Importantly, cosolvent simulations revealed the highly dynamic nature of the hydrophobic binding pockets in Bcl-xL and yielded new structural insights for the design of novel Bcl-xL small-molecule inhibitors.

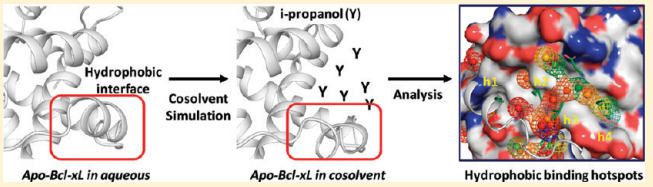

KEYWORDS: Protein−protein interfaces, Bcl-xL protein, cosolvent molecular dynamics simulation

Protein−protein interactions (PPIs) play a key role in regulating many cellular processes.[1] Common features for many PPIs include their relatively large interface[2] and the high plasticity observed at the protein−protein interface.[3] Both features make the design of nonpeptide, small-molecule inhibitors to block PPIs a difficult task despite major progress made in recent years for several PPIs.[4] Although a protein−protein interface can be large, an emerging concept is that the binding free-energy (binding affinity) between the binding partners is often dominated by a few key "hot spots".[5] An in-depth knowledge of the hot spots is useful not only for understanding the functions of proteins but also for the design of nonpeptide small-molecule inhibitors of protein−protein interactions.

In this study, we have investigated the use of molecular dynamic (MD) simulations in a cosolvent environment to identify and analyze the "hot spots" in the Bcl-xL protein. Bcl-xL is a key antiapoptotic regulator and a member of the Bcl-2 family of proteins.[6] Bcl-xL has 233 amino acids and is a mainly α helix protein in which its C-terminal helix inserts into intracellular membranes including mitochondria. Bcl-xL inhibits apoptosis by heterodimerization with pro-apoptotic Bcl-2 proteins, such as Bad, Bim, and Bax proteins.[6] The interactions between Bcl-xL and its binding partners are mediated by a large, hydrophobic groove in Bcl-xL and the BH3 (Bcl-2 Homology 3) domain of these proteins. The Bcl-xL protein is investigated for several reasons: (1) Bcl-xL interacts with its binding partners through a large, primarily hydrophobic binding groove.[7] (2) Bcl-xL undergoes unfolding and refolding in its binding groove when bound to its binding partners with respect to its apo-form, and such large and extensive conformational changes expose a number of buried hydrophobic residues for effective interaction with its binding partners. (3) The interactions of Bcl-xL with its binding partners are dominated by a few key hydrophobic residues and one charged residue, hence a few "hot spots" based upon crystal structures and biochemical data.[8] (4) There are intense research efforts[9] toward the design of potent, nonpeptide, small-molecule inhibitors of Bcl-xL, and one such compound (ABT-263) has been advanced into clinical development.[10] (5) A number of high-resolution crystal structures are available for Bcl-xL alone (the apo-form) and in complex with peptide-based and nonpeptide inhibitors.[8,11−14]

Cosolvents are frequently used to solubilize proteins. In the experimental multiple solvent crystal structures (MSCS) approach,[15] they were used to locate potential protein binding sites. The MSCS method soaks the protein crystals in different cosolvent concentrations, allowing the cosolvent molecules to diffuse to different protein binding sites. Although highly elevated concentrations of organic solvents in water can induce unfolding of a protein, hen egg-white lysozyme remains stable in its native conformation and can be cocrystallized at 16−24% of cosolvent concentrations.[16] Up to 60% of three different cosolvent concentrations have been used to stabilize the dynamic switch II in the H-Ras protein for crystal structure determination.[17] Four different ratios of methanol, DMSO, and

Received: November 22, 2010
Accepted: January 5, 2011
Published: January 13, 2011

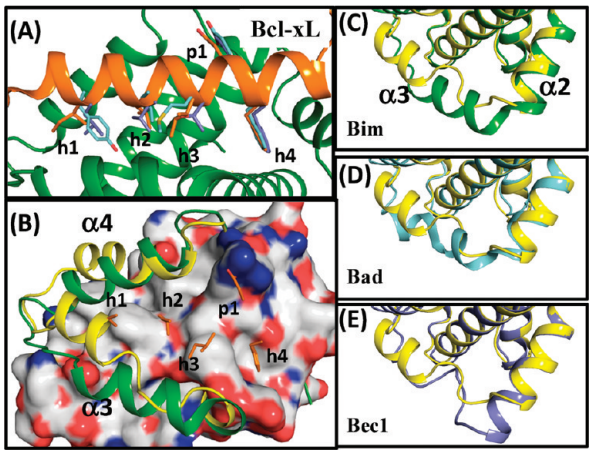

Figure 1. (A) Superimposition of Bcl-xL with the Bim (orange), Bad(cyan), and Bec1 (blue) BH3 peptides. (B) Structural alignment between the ligand-free Bcl-xL(yellow) and Bcl-xL with the Bim peptide(green). H1-4 and p1 residues of the Bim peptide are shown in orange. Conformational changes of the α3 helix in Bcl-xL when binding to (C) Bim (green), (D) Bad (cyan), and (E) Bec1 (blue) peptide. The reference structure of ligand-free Bcl-xL is shown in yellow. The PyMOL program (www.pymol.org) was used to view the protein models and prepare the graphics.

water cosolvent systems were used to study the dynamic transition of xylanase experimentally.[18] Recently, Barril and co-workers[19] investigated the maximum binding affinity of the binding sites in five different proteins by performing MD simulations of proteins in a 20% v/v isopropanol/water environment. We have recently shown[20] that the binding free energy of the isopropanol in the binding site of thermolysin obtained using the cosolvent simulation is comparable to the values determined by the double decoupling method.[21] In the present study, we used the same 20% v/v isopropanol/water condition for our cosolvent simulation of the Bcl-xL system.

In addition to the apo structure, crystal structures of Bcl-xL with several peptides derived from Bcl-2 homology domain 3 (BH3) of pro-apoptotic Bcl-2 proteins and with nonpeptide small-molecule inhibitors have been determined. These include complexes with the wild type BH3 domains of Bak,[22] Bad,[23] Bim,[11,12] Beclin-1(Bec1),[13] mutated BH3 domain peptides,[14] foldamer peptides,[12] and small molecule inhibitors.[8] These crystal structures have revealed that when bound to BH3 peptides, Bcl-xL undergoes substantial backbone conformational changes at the α3 and α4 helices and significant changes at the α2 and α7 helices (cf. Figure 1C−E and S2). Unfolding of α3 in Bcl-xL is seen in the Bad- and Bec1-bound structures, and an additional helical turn at the end of α2 is observed in the Bec1-bound conformation. The backbone changes in the flexible α3 helix in Bcl-xL expose a large hydrophobic groove, which is used in binding to the amphipathic, helical BH3 domain peptides consisting of 20−25 amino acid residues.

MD simulations were performed on the apo-Bcl-xL structure in water and in cosolvent to understand the effects of the cosolvent molecules on the energetics and conformations of the protein. The molecular mechanics Poisson−Boltzmann surface area (MM-PBSA) model[24] was used to calculate and compare the conformational free energy ($\Delta G^{\text{MM-PBSA}}$) of Bcl-xL using conformations obtained from simulation trajectories in water and cosolvent. This comparison allows us to determine the energetic perturbation to the Bcl-xL conformations simulated in the cosolvent environment. Throughout the 32 ns simulations, the average $\Delta G^{\text{MM-PBSA}}$ of the apo-Bcl-xL in cosolvent is similar to that in water (−1575 ± 29 in cosolvent versus −1581 ± 30 kcal/mol in water) (Figure S3D). However, conformations of the apo-Bcl-xL in cosolvent give higher surface accessible areas (ASAs) than those in water (8336 versus 7796 Å^2). According to the PB solvation model, the differences of ASAs for the apo-Bcl-xL conformations in two different media contribute 3.89 kcal/mol in nonpolar solvation. Although the backbone rmsd of the apo-Bcl-xL (α2-α7) is maintained at 1.5 Å in both simulations, there are significant differences with respect to conformational changes between the two simulations. In cosolvent, the α3 and α4 helices of Bcl-xL undergo large conformational changes starting at 16 ns and become stabilized after 20 ns. In water, only minor backbone changes are found in the apo-Bcl-xL conformations. The conformations of the apo-Bcl-xL in cosolvent at 16 and 32 ns are shown in Figure S4C and D of the Supporting Information. Both figures indicate that interaction between the isopropanol and the apo-Bcl-xL drives the apo-Bcl-xL into a conformational state in which the buried h1 and h2 sites become exposed. In contrast, both sites remain buried in the conformations of apo-Bcl-xL throughout 32 ns of simulations in water (Figure S4A and B). Differences in the per residue ASA calculations of hydrophobic residues at the binding site identified greater surface exposure in Y101, A104, F105, L108, I114, and L130 (>10 Å^2), involving primarily the α3 helix in the conformations obtained from cosolvent simulations (Figure S5B). Exposure of these residues, except Tyr101, is also seen when comparing three peptide-bound structures and the Apo-Bcl-xL structure (Figure S5A). Our simulations show that while the cosolvent molecules cause only small energetic perturbation, they induce significant backbone conformational changes in the α3 helix of the apo-Bcl-xL, exposing the h1 and h2 sites, similar to that observed in the crystal structures of Bcl-xL bound to different binding partners.

We next performed MD simulations of three different peptide-bound Bcl-xL crystal structures shown in Figure 1C but with the BH3 peptides removed from the structures (holo-Bcl-xL structures). In pure water simulations, the Bim-bound Bcl-xL structure remains in a conformational state with an intact α3 helix (Figure 2A); the Bad-bound Bcl-xL structure refolds its partially distorted α3 helix during the 32 ns simulation (Figure 2B); the Bec1-bound Bcl-xL structure partially loses its helicity for its α2 and α4 segments (Figure 2C). In all three simulations in water, a number of exposed hydrophobic residues in the binding groove become reburied and result in a conformational state, similar to the crystal structure of apo-Bcl-xL.

In the cosolvent simulations, small backbone changes in the Bim-bound holo Bcl-xL structure are observed (Figure 2D) while the Bec1-bound holo Bcl-xL structure remains stable (Figure 2F). In the case of the Bad-bound holo Bcl-xL structure, there is a large conformational change with respect to the region consisting of the tail of α2 and the whole α3 helix segments (F95−P116) (Figure 2E). However, in all cases, the three holo-Bcl-xL conformations maintain their exposed hydrophobic surface in the binding groove in the cosolvent simulations, in contrast to that observed in pure water simulations. Comparison of the ASAs of the hydrophobic residues around the binding site (A93−V155) between conformations obtained from both solvent media show that F97, F105, L108, L112, Y120, V126, and L130 are indeed more exposed to solvent in the cosolvent simulation than in water (Figure S5C). These residues are even more exposed when Bcl-xL binds to BH3 peptides (cf. Figure S5A and C).

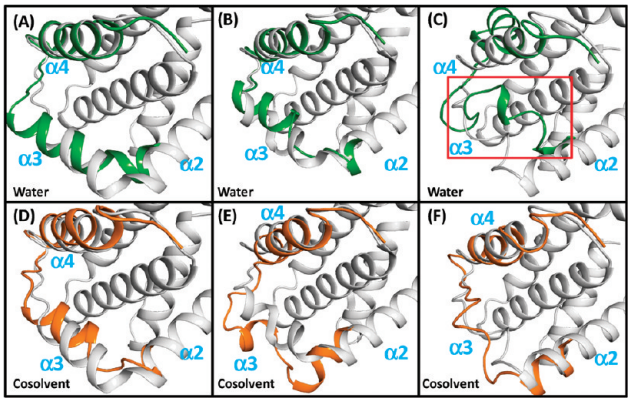

Figure 2. Comparison of the crystal structures of the Bim-bound (A, D), the Bad-bound (B, E), and the Bec1-bound (C, F) Bcl-xL with snapshots of conformations after 32 ns simulations. Conformations of crystal structures; snapshots in water and in cosolvent are colored in gray, green, and orange. Only residues F97−N136 in the snapshots are shown for clarity.

Energetically, the $\Delta G^{\text{MM-PBSA}}$ values of the holo-Bcl-xL conformations obtained in water and cosolvent are similar (−1586 versus −1605 kcal/mol for the Bim-bound, −1612 versus −1623 for the Bad-bound, and −1616 versus −1607 kcal/mol for the Bec1-bound). Although ASAs in the Bad-bound and Bec1-bound Bcl-xL conformations obtained in cosolvent are greater than those obtained in water, only small differences are found in the Bim-bound Bcl-xL conformations simulated in both media.

We next identified the hydrophobic hot spots using the cosolvent mapping method based on an ensemble of protein conformations obtained from the cosolvent simulations. In the cosolvent mapping method, the binding site of Bcl-xL is probed by atoms of the cosolvent molecules *via* their interaction with the protein. The observed frequency (N_p) of the probe atom at a grid point around the protein binding site is compared with an expected frequency (N_0) in a cosolvent mixture to give an estimate of the binding free energy of the probe atom at that grid point, i.e. $\Delta G^{\text{CM}} = -kT \log (N_p/N_0)$. Grid points with binding free energies higher than −0.83 kcal/mol were collected to form pseudoatoms (vertices with a radius = 1.4 Å), and a bonding distance of 2.5 Å between pseudoatoms (edge) was used to generate chemical graphs (details in Supporting Information). The derived chemical graphs represent the hot spots, whose specific physical properties depend on the types of probe atoms used. Here, the carbon atoms of the terminal methyl groups in isopropanol were used as probes to identify the hydrophobic hot spots in Bcl-xL.

Figure 3 shows the hydrophobic hot spots determined on the basis of conformations obtained from the 32 ns MD simulations in cosolvent for one apo-Bcl-xL and three holo-Bcl-xL structures. The relative rigidity of the α3 helix of the Bim-bound conformations yields a distribution of the hydrophobic hot spots covering the helical backbone of the Bim peptide and the h2 and h4 sites (Figure 3B). Differences in the conformational changes of the α3 helix in Bcl-xL in its binding with the Bad and Bec1 peptides are also reflected on the distribution of hot spots (Figure 3C and D). Hydrophobic hot spots determined by the Bad-bound Bcl-xL are skewed toward the h2 and h3 sites and less toward the h4 site. In contrast, the hot spots are distributed more toward the h3 and h4 sites and less deeply into the h2 site in the Bec1-bound Bcl-xL. Hot spots are mainly found at the h2, h3, and h4 sites from the

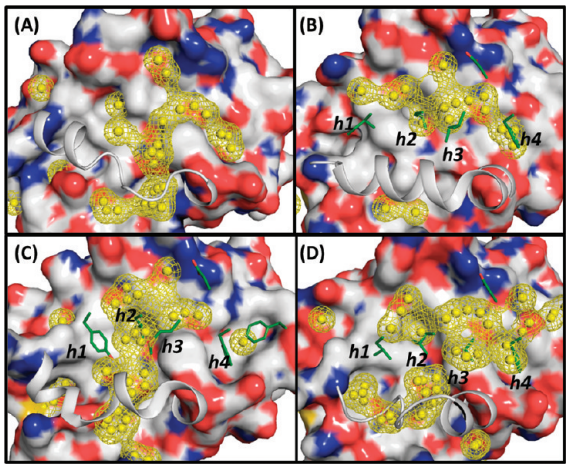

Figure 3. Hydrophobic hot spots (yellow balls) in the BH3 peptide binding groove detected from the cosolvent mapping method based on 32 ns of simulations. (A−D) Results using the apo-, Bim-bound, Bad-bound, and Bec1-bound Bcl-xL conformations, respectively. Four conserved hydrophobic residues and one acidic residue are shown in the stick model. Crystal structures of each conformation are used as the reference. The α3 helix is shown without the surface rendering for clarity.

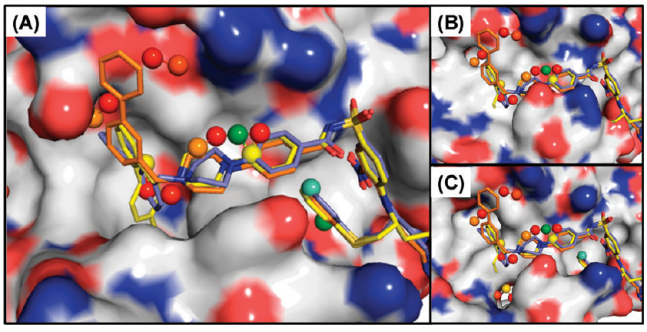

Figure 4. Alignment of the hydrophobic hot spots (*pseudo*-carbon atoms) determined from the conformations of the apo-Bcl-xL simulated in cosolvent with the crystal structures of Bcl-xL with ABT737 (yellow, PDB ID: 2YXJ) and conformation 1 (blue) and 2 (orange) of W1101542 (PDB ID: 3INQ). The red pseudoatoms yield lower binding affinity than the orange, yellow, green, and cyan ones. Bcl-xL is shown in surface representation. The reference protein structures are (A) the ABT737-bound Bcl-xL crystal structure and (B and C) the apo-Bcl-xL conformation (B) in water and (C) in cosolvent at 32 ns of MD simulation.

apo-Bcl-xL simulation (Figure 3A), and additional hot spots situated more deeply in the protein are seen at the h2 and h3 sites. The locations of these hot spots are consistent with key components of either the Bcl-xL inhibitors ABT737 or W1101542, as seen in their crystal structures (Figure 4A). The conformation of apo-Bcl-xL obtained from the 32 ns cosolvent simulation gives an example that the binding site is better defined and suitable for small molecules than the conformation obtained from the 32 ns water simulation (cf. Figure 4B and C). A comparison of the hot spots distribution in the four different Bcl-xL conformations reveals a narrower consensus region covering predominantly the h2, h3, and h4 sites. Our hot spot analysis suggests that different scaffolds of small molecules of Bcl-xL may be designed to target different conformations of Bcl-xL.

Our analysis also reveals the conformational dependence of the distribution of hot spots for Bcl-xL. Dynamical changes of the

dx.doi.org/10.1021/ml100276b |*ACS Med. Chem. Lett.* 2011, 2, 280–284

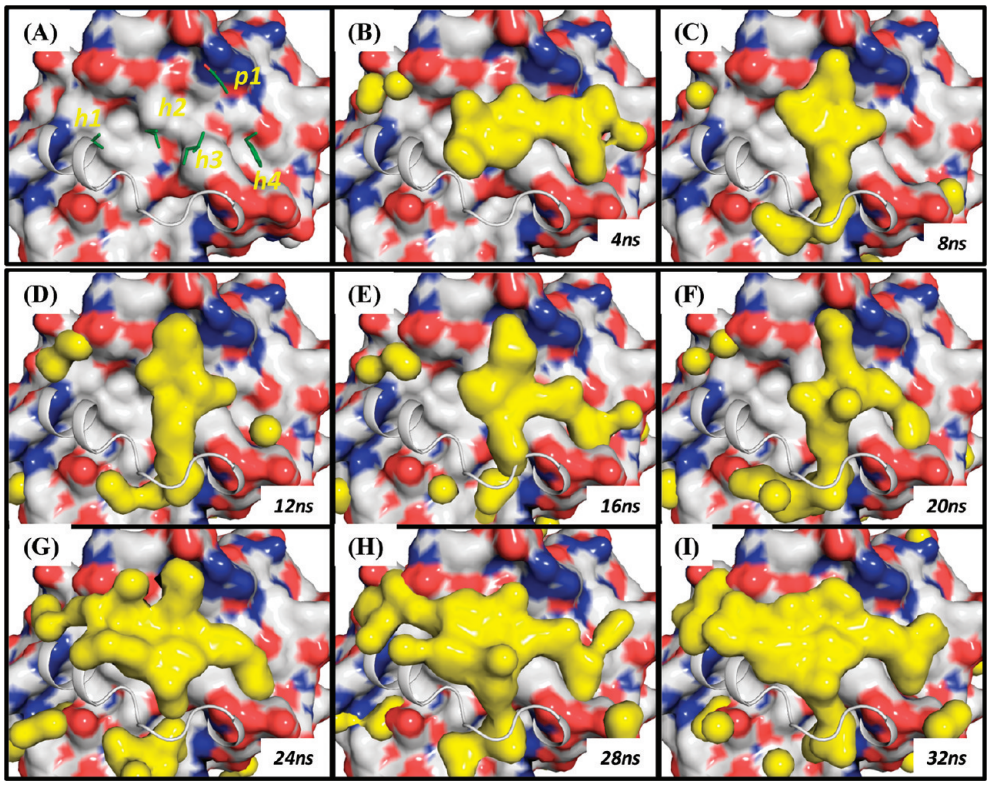

Figure 5. Evolution of hot spots (contour surface) every 4 ns determined from the cosolvent simulation started with the apo form of the Bcl-xL crystal structure. The Bim BH3 peptide is aligned, and key residues are green.

binding site conformations can be clearly seen with different hydrophobic hot spot patterns based on the conformations of the apo-Bcl-xL in every 4 ns window from the 32 ns cosolvent simulations in Figure 5. Initially, hot spots cluster at the h2, h3, and h4 sites in the first 20 ns of the simulation (Figure 5B−F). After 20 ns of simulation, additional hot spots spreading to the h1 site emerge as a result of the backbone conformational changes in the α3 helix (cf. Figure S3A).

In summary, we have analyzed the Bcl-xL binding groove through MD simulations in pure water and in isopropanol/water cosolvent and hot spot mapping. When simulations are performed in water, the binding site of the apo-Bcl-xL has relatively minor conformational changes. Simulations of three holo-Bcl-xL structures in water show that the protein undergoes significant conformational changes and results in burying of several solvent-exposed hydrophobic residues in the binding groove, which are critical for effective interactions with the binding partners of Bcl-xL. In contrast, in the cosolvent, the apo-Bcl-xL structure has undergone large conformational changes, exposing large hydrophobic surfaces at the interface, which is similar to that observed in the crystal structures of Bcl-xL in complex with its peptide and nonpeptide ligands. Three holo-Bcl-xL structures retain their exposed hydrophobic surface throughout the 32 ns simulations, although there are significant conformational changes with respect to one segment in the Bad-bound holo Bcl-xL structure. Despite the substantial structural differences, the free energy differences of the Bcl-xL conformations obtained in both media are small, and they probably reflect the small perturbation by the cosolvent molecules and the plasticity of Bcl-xL. Hydrophobic hot spots determined using four different simulations in cosolvent reveal the high plasticity of the Bcl-xL binding sites. Importantly, hot spots determined based on the apo-Bcl-xL conformation are consistent with pharmacophore elements of known nonpeptide, small-molecule inhibitors. Furthermore, our simulations also reveal additional binding hot spots not found in the crystal cocomplex structures, which can be used for the design of novel and potent small-molecule inhibitors of Bcl-xL. Taken together, our present study suggests that cosolvent MD simulation is highly effective to investigate biologically relevant conformations for flexible and hydrophobic binding sites in proteins and is capable of yielding new structural insights not found in the crystal structures. We are currently employing this approach for investigation of other protein−protein interactions, which also possess highly flexible and hydrophobic binding sites.

■ ASSOCIATED CONTENT

Supporting Information. Details of the computational methods. This material is available free of charge via the Internet at http://pubs.acs.org.

■ AUTHOR INFORMATION

Corresponding Author

*Telephone: +1 734 6150362. Fax:+1 734 6479647. E-mail: shaomeng@umich.edu.

■ ACKNOWLEDGMENT

We thank Dr. George W. A. Milne for his critical reading of the manuscript.

■ REFERENCES

(1) Aloy, P.; Russell, R. B. *Nat. Rev. Mol. Cell Biol.* **2006**, *7*, 188.
(2) Wells, J. A.; McClendon, C. L. *Nature* **2007**, *450*, 1001.

(3) Winget, J. M.; Mayor, T. *Mol. Cell* **2010**, *38*, 627.
(4) Fry, D. C. *Pept. Sci.* **2006**, *84*, 535.
(5) Wells, J. A. *Proc. Natl. Acad. Sci. U.S.A.* **1996**, *93*, 1.
(6) Youle, R. J.; Strasser, A. *Nat. Rev. Mol. Cell. Biol.* **2008**, *9*, 47.
(7) Petros, A. M.; Olejniczak, E. T.; Fesik, S. W. *Biochim. Biophys. Acta* **2004**, *1644*, 83.
(8) Lee, E. F.; Czabotar, P. E.; Smith, B. J.; Deshayes, K.; Zobel, K.; Colman, P. M.; Fairlie, W. D. *Cell Death Differ.* **2007**, *14*, 1711.
(9) Reed, J. C.; Pellecchia, M. *Blood* **2005**, *106*, 408.
(10) Tomillero, A.; Moral, M. A. *Methods Find. Exp. Clin. Pharmacol.* **2008**, *30*, 761.
(11) Liu, X.; Dai, S.; Zhu, Y.; Marrack, P.; Kappler, J. W. *Immunity* **2003**, *19*, 341.
(12) Lee, E. F.; Sadowsky, J. D.; Smith, B. J.; Czabotar, P. E.; Peterson-Kaufman, K. J.; Colman, P. M.; Gellman, S. H.; Fairlie, W. D. *Angew. Chem., Int. Ed. Engl.* **2009**, *48*, 4318.
(13) Oberstein, A.; Jeffrey, P. D.; Shi, Y. *J. Biol. Chem.* **2007**, *282*, 13123.
(14) Lee, E. F.; Czabotar, P. E.; Yang, H.; Sleebs, B. E.; Lessene, G.; Colman, P. M.; Smith, B. J.; Fairlie, W. D. *J. Biol. Chem.* **2009**, *284*, 30508.
(15) Mattos, C.; Ringe, D. *Nat. Biotechnol.* **1996**, *14*, 595.
(16) Deshpande, A.; Nimsadkar, S.; Mande, S. C. *Acta Crystallogr., D: Biol. Crystallogr.* **2005**, *61*, 1005.
(17) Buhrman, G.; de Serrano, V.; Mattos, C. *Structure* **2003**, *11*, 747.
(18) Reat, V.; Dunn, R.; Ferrand, M.; Finney, J. L.; Daniel, R. M.; Smith, J. C. *Proc. Natl. Acad. Sci. U.S.A.* **2000**, *97*, 9961.
(19) Seco, J.; Luque, F. J.; Barril, X. *J. Med. Chem.* **2009**, *52*, 2363.
(20) Yang, C.-Y.; Wang, S. *ACS Med. Chem. Lett.* **2010**, *1*, 125.
(21) Gilson, M. K.; Given, J. A.; Bush, B. L.; McCammon, J. A. *Biophys. J.* **1997**, *72*, 1047.
(22) Sattler, M.; Liang, H.; Nettesheim, D.; Meadows, R. P.; Harlan, J. E.; Eberstadt, M.; Yoon, H. S.; Shuker, S. B.; Chang, B. S.; Minn, A. J.; Thompson, C. B.; Fesik, S. W. *Science* **1997**, *275*, 983.
(23) Petros, A. M.; Nettesheim, D. G.; Wang, Y.; Olejniczak, E. T.; Meadows, R. P.; Mack, J.; Swift, K.; Matayoshi, E. D.; Zhang, H.; Thompson, C. B.; Fesik, S. W. *Protein Sci.* **2000**, *9*, 2528.
(24) Kollman, P. A.; Massova, I.; Reyes, C.; Kuhn, B.; Huo, S.; Chong, L.; Lee, M.; Lee, T.; Duan, Y.; Wang, W.; Donini, O.; Cieplak, P.; Srinivasan, J.; Case, D. A.; Cheatham, T. E. *Acc. Chem. Res.* **2000**, *33*, 889.

Supporting Information

Analysis of Hydrophobic Binding Hotspots of Highly Flexible Bcl-xL Protein-Protein Interfaces by Cosolvent Molecular Dynamics Simulation

*Chao-Yie Yang, and Shaomeng Wang**

Departments of Internal Medicine, Pharmacology and Medicinal Chemistry, University of Michigan, 1500 E. Medical Center Drive, Ann Arbor, MI 48109, USA

* Corresponding author: Email: shaomeng@umich.edu; Phone:+1 734 6150362; Fax:+1 734 6479647.

Methods and Calculations

Preparation of molecular dynamic simulation

Crystal structures of one apo-Bcl-xL, three Bcl-xL, and the BH3 domain peptides taken from the Protein Databank[1] were used in this study. The PDB IDs for them are, 1MAZ, 3FDL (with the Bim BH3 peptide), 2BZW (with the Bad BH3 peptide) and 2P1L (with the Bec1 BH3 peptide). Because a loop segment connecting the α1 and the α2 helix (naming see Figure S1) are missing in all available crystal structures, we capped the C-terminus of α1 and the N-terminus of α2 with the N-methyl group (NME) and the acetyl group (ACE), respectively, to mimic the backbone of the missing flexible loop. The sequences of Bcl-xL in 1MAZ, 3FDL and 2P1L are for human while that in 2BZW is for mouse. To make the same comparison between the Bad-bound and Bec1-bound Bcl-xL conformations, we made two mutations at A168S and E193D. The Bcl-xL protein used in our simulations consists of 139 residues (S4—S25-NME, ACE-S83—N197) with the sequence:

SNRELVVDFLSYKLSQKGYSWS-(NME), (ACE)-SEAVKQALREAGDEFEL RYRRAFSDLTSQLHITPGTAYQSFEQVVNELFRDGVNWGRIVAFFSFGGALCVES VDKEMQVLVSRIAAWMATYLNDHLEPWIQENGGWDTFVELYGN.

In preparation of the simulations, we have used the PROPKA[2-3] to determine the protonation state of ionizable groups on Bcl-xL. We found all the titratable groups should be charged according to standard physiological conventions. PMEMD from Amber (version 10)[4] was used for molecular dynamics simulations. The Amber 99SB force field parameters[5] were used for the amino acids.

Pure water solvent simulations

To prepare the topology and coordinate files, counter ions were added to neutralize the charges in Bcl-xL before it was placed in a 13Å octahedral box of water. The TIP3P[6] water model was used. A 3000-step minimization (steps 1-1000 using conjugated gradient followed by 2000 steps steepest decent) was first carried out. After minimization, a 500 ps constant volume and constant temperature (NVT) simulation was performed to raise the temperature of the system to 298K while constraining backbone atoms with a 5 kcal/mol/Å^2 force constant with reference to the crystal structure. A second 200 ps constant pressure and constant temperature (NPT) simulation at 298 K was performed while constraining backbone atoms with a 2 kcal/mol/Å^2 force constant with reference to the crystal structure. The system was then equilibrated for 1 ns at 298K without any constraints. The system is then ready for the 32 ns production run. All the MD simulations were in the isobaric isothermal (NPT, T = 298K and P = 1 atm) ensemble. The SHAKE[7] algorithm was used to fix bonds involving hydrogen. The PME method[8] was used and the non-bonded cutoff distance was set at 10Å. The time step was 2 fs, and neighboring pairs list was updated every 20 steps. A 32 ns MD simulation of the 139 amino acids Bcl-xL required 24 days of four dedicated dual core dual AMD 2.0 GHz processors nodes in our cluster. Advances in computing facility should relieve the limitation of this approach to study larger protein systems and allow investigating dynamical motions proteins at a longer timescale.

Cosolvent mapping simulations and analyses

An equilibrated cosolvent box (20% v/v isopropanol in water) was provided by Dr. Barril. For MD simulations, the structure of Bcl-xL was first neutralized with counter

ions and placed in a 13Å octahedral box of the cosolvent system. After a 3000-step minimization, a series of equilibration protocols were used as follows:

1. 50 ps, NVT, temperature changes from 0 to 298 K, all heavy atoms of proteins were constrained with a 5 kcal/mol/Å^2 harmonic force constant.
2. 50 ps, NPT, temperature changes from 298 to 350 K, all heavy atoms of proteins were constrained with a 1 kcal/mol/Å^2 harmonic force constant.
3. 50 ps, NPT, temperature changes from 400 to 450 K, all heavy atoms of proteins were constrained with a 1 kcal/mol/Å^2 harmonic force constant.
4. 50 ps, NPT, temperature changes from 450 to 500 K, all heavy atoms of proteins were constrained with a 1 kcal/mol/Å^2 harmonic force constant.
5. 50 ps, NPT, temperature changes from 500 to 550 K, all heavy atoms of proteins were constrained with a 1 kcal/mol/Å^2 harmonic force constant.
6. 100 ps, NPT, temperature kept at 550 K, all heavy atoms of proteins were constrained with a 1 kcal/mol/Å^2 harmonic force constant.
7. 50 ps, NPT, temperature changes from 550 to 425 K, all heavy atoms of proteins were constrained with a 1 kcal/mol/Å^2 harmonic force constant.
8. 50 ps, NPT, temperature changes from 425 to 298 K, all heavy atoms of proteins were constrained with a 1 kcal/mol/Å^2 harmonic force constant.
9. 1 ns, NPT, temperature kept at 298K.

The Procheck program[9-10] was used to examine the backbone dihedral angles of the protein conformations after step 8. The corresponding Ramachandran plots for the apo- and three holo-Bcl-xL conformations were shown in Figure S6. More than 89 % of the amino acids in Bcl-xL have dihedral angles in favored regions except Ser23 and Trp24

(S20 and W21 in Figure S6) in the apo-Bcl-xL. Both amino acids are at the end of NME-cap and located at the back side of the binding site. The deviations of their backbone dihedral angles from favored regions may be attributed to the unresolved loop segment in the crystal structures which were not included in our simulations. A production simulation of 32 ns at 298K was performed. Snapshots of the whole system were taken at intervals of 2 ps.

The hotspot analyses are similar to those reported by Barril et. al.[11] but with our own implementation.[12] They are as follows. Conformations of Bcl-xL from the 32 ns simulation were aligned first along the α5 helix and the cosolvents were imaged into an octahedral box. Evenly spaced 0.5Å grids covering the entire Bcl-xL molecule were created and the counts of the probe atoms in isopropanol (terminal carbon or hydroxyl oxygen atoms) occupying each grid point were calculated. These calculations were performed using the ptraj program from Amber suite. After normalizing the counts of the probe atoms occupying each grid point (N_p), an empirical formula:

$$\Delta G^{CM} = - kT \log (N_p/N_0), \quad (S1)$$

where k is the Boltzman constant, T is room temperature and N_0 is the counts of the probe atoms occupying any grid point (expected occupancy) in 20% v/v cosolvent box without a protein. The N_0 values for terminal carbon and hydroxyl oxygen atoms were provided by Dr. Barril. Based on the values of ΔG, only the grids calculated to be lower than -0.83 kcal/mol were kept for the next analysis. A search procedure was used to find the grid point with the lowest ΔG value and grid points within 1.4 Å of this grid point were removed. The same procedure continued until all grid points were visited. Results of this procedure give *pseudo* atoms in a space. A cluster analysis based on a Depth First

Search (DFS) algorithm with a criterion of two *pseudo* atoms being connected within 2.5 Å was implemented in a C++ program to generate chemical graphs. In analogy to the graph theory, pseudo atoms are vertices and bonds are edges. These chemical graphs form the bases of hotspots probes and were reported in Figure 3 and 4.

Conformational free energy calculations

Bcl-xL conformations were extracted every 100 ps from the simulations in either water or cosolvent. The conformational free energy of Bcl-xL was calculated using the MM-PBSA method with the equation,

$$\Delta G^{MM\text{-}PBSA} = E_{MM} + G_{solv} - TS, \qquad \text{(S2)}$$

where E_{MM} is the molecular mechanics energy, G_{solv} is the solvation free energy and S is the entropy for the protein. The PBradii was set to mbondi2 in the topology file for the solvation free energy calculation. In the normal mode calculations, a distance-dependent dielectric constant $\varepsilon = 4r$ was used, the maximum cycle was set to 60,000, and the convergence tolerance was 0.0002 kcal $mol^{-1}Å^{-1}$.

Figure S1 Sequence alignment of the BH3 domain of BH3 proteins that bind with the Bcl-2 family of proteins. Key hydrophobic residues are denoted h1-4 and p1 is the conserved polar residue. These five residues contribute predominantly to the binding between the BH3 domain peptides and Bcl-2 proteins

Protein								h1				h2			h3		p1		h4						
mBIM		D	L	R	P	E	I	R	I	A	Q	E	L	R	R	I	G	D	E	F	N	E	T	Y	T	R	R
Bim	81-106	D	M	R	P	E	I	W	I	A	Q	E	L	R	R	I	G	D	E	F	N	A	Y	Y	A	R	R
Puma	130-155	E	E	Q	W	A	R	E	I	G	A	Q	L	R	R	M	A	D	D	L	N	A	Q	Y	E	R	R
mBmf	128-151		H	R	A	E	V	Q	I	A	R	K	L	Q	C	I	A	D	Q	F	H	R	L	H	T	Q	
Bad	103-128	N	L	W	A	A	Q	R	Y	G	R	E	L	R	R	M	S	D	E	F	V	D	S	F	K	K	G
Bik	51-75		M	E	G	S	D	A	L	A	L	R	L	A	G	I	G	D	E	M	D	V	S	L	R	A	P
Hrk	26-51	R	S	S	A	A	Q	L	T	A	A	R	L	K	A	I	G	D	E	L	H	Q	R	T	M	W	R
Bid	81-104			D	I	I	R	N	I	A	R	H	L	A	Q	V	G	D	S	M	D	R	S	I	P	P	G
Noxa	18-43	P	A	E	L	E	V	E	C	A	T	Q	L	R	R	F	G	D	K	L	N	F	R	Q	K	L	L
Beclin-1	105-130	G	S	G	T	M	E	N	L	S	R	R	L	K	V	T	G	D	L	F	D	I	M	S	G	Q	T

Figure S2. Number convention of the helices in Bcl-xL.

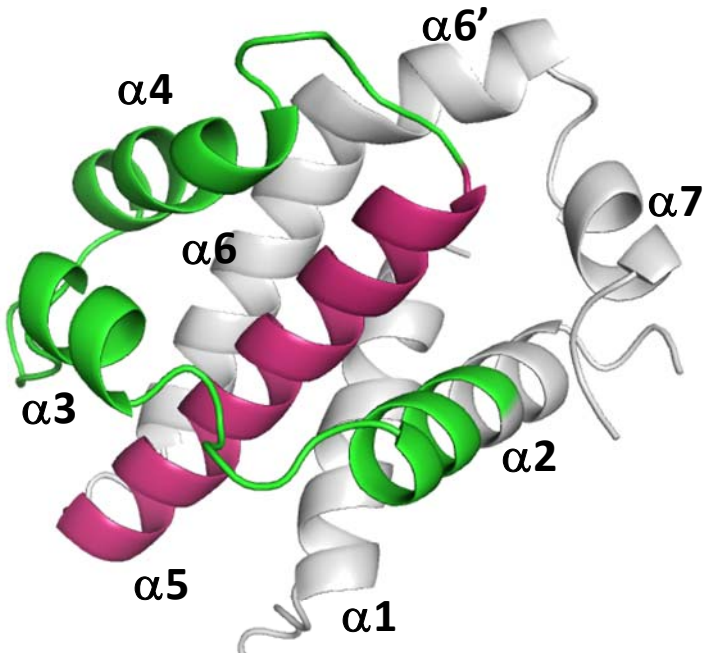

Figure S3. Calculated backbone RMSD of the Bcl-xL conformations simulated in the water (black) and the cosolvent (red). The reference conformation is the crystal structure of apo Bcl-xL. Alignment of the α5 helix (seq. W137-K157) was undertaken before calculating the RMSD of the α5 helix (B) and the α3 plus α4 (seq. A93-W137) (A). (C) is the RMSD of all amino acids after alignment. The total free energy (ΔG) and the accessible surface area (ASA) calculated using the MM-PBSA method are in (D) and (E). The units used are kcal/mol.

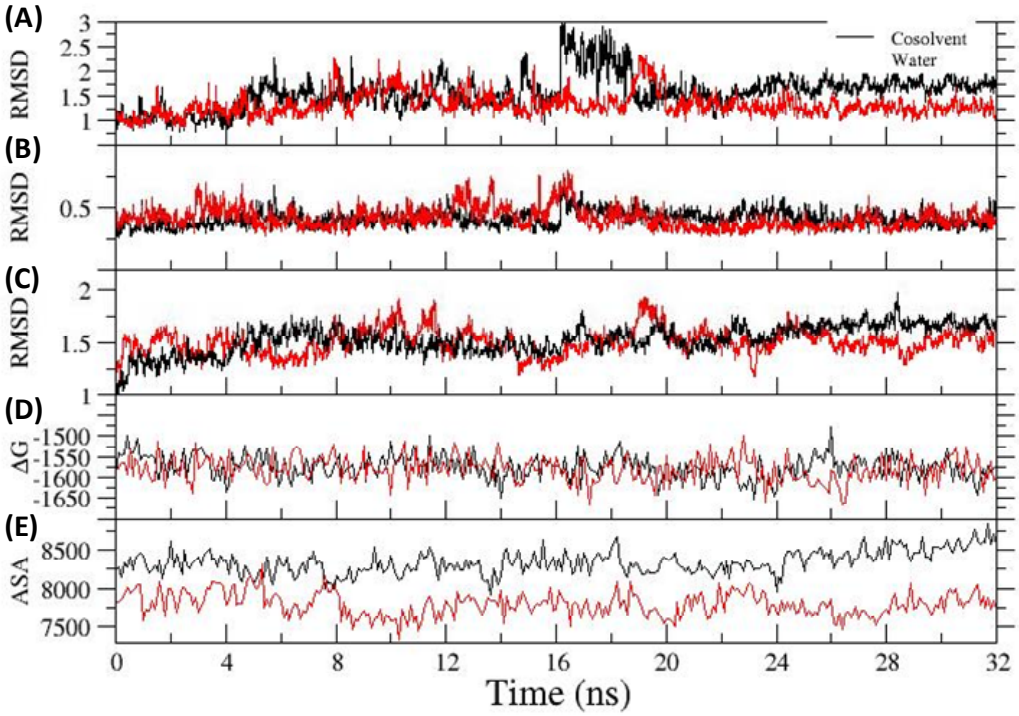

Figure S4. (A) Comparison of the conformation of the crystal structure (grey) and snapshot of Bcl-xL at 32 ns in pure water (cyan). The surface representation of Bcl-xL (B) at 32 ns in pure water simulations; (C) at 16 ns and (D) at 32 ns in the cosolvent simulation. Bim BH3 peptide was aligned and residues interacting with Bcl-xL were shown by the green stick model.

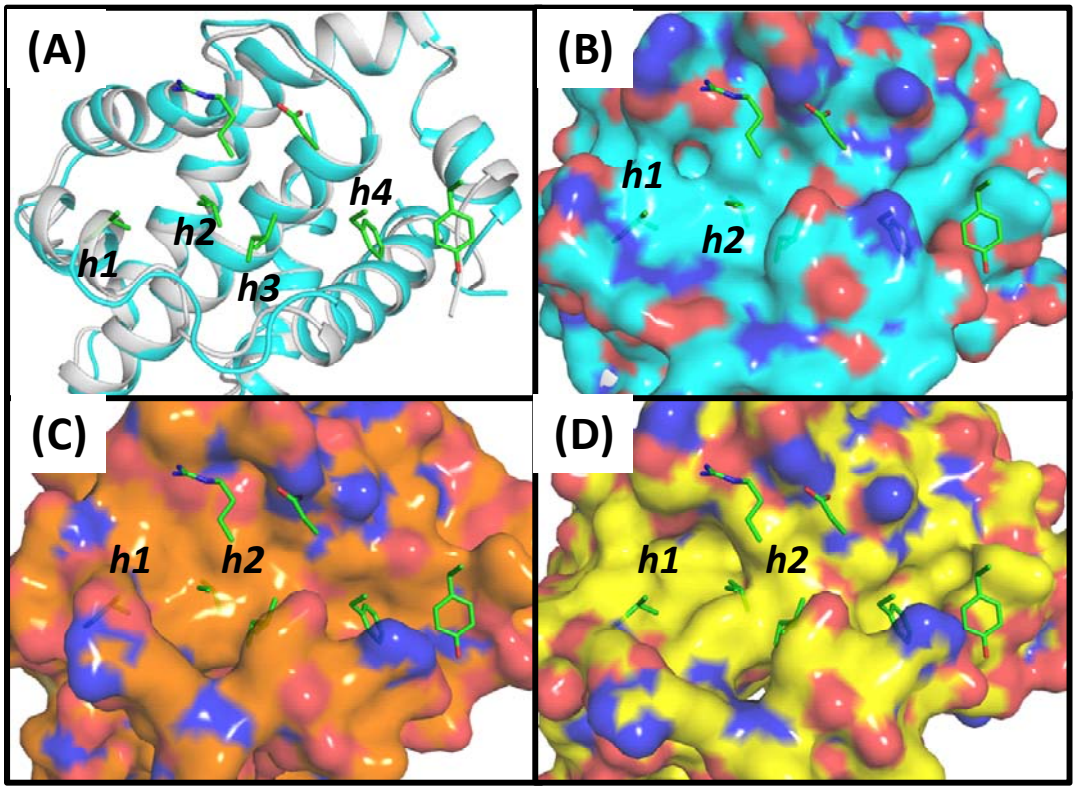

Figure S5. Accessible surface area differences (ΔASA) of hydrophobic residues (including Tyr) around the binding site of Bcl-xL. (A) Between the Bim-(blue), Bad-(red), Bec1- (green) bound and Apo Bcl-xL crystal structures. (B-C) Between conformations obtained from 32 ns cosolvent and aqueous simulations. Positive ΔASA corresponds to exposure whereas negative buried. α2-α5 helices are labeled on top.

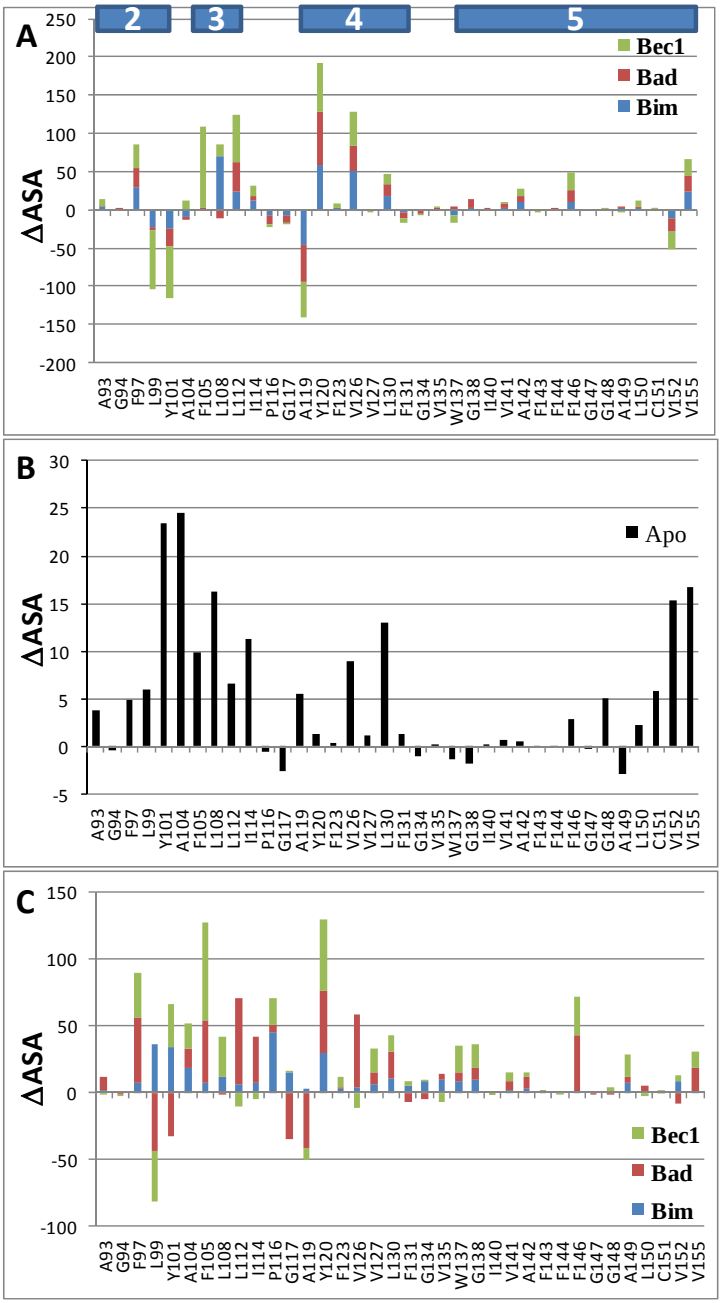

Figure S6. Ramachandran plots using the apo-Bcl-xL in the crystal structure, the apo-Bcl-xL conformation in the water environment, the apo-Bcl-xL and three holo-Bcl-xL conformations in the cosolvent environment after step 8 in the simulation preparation.

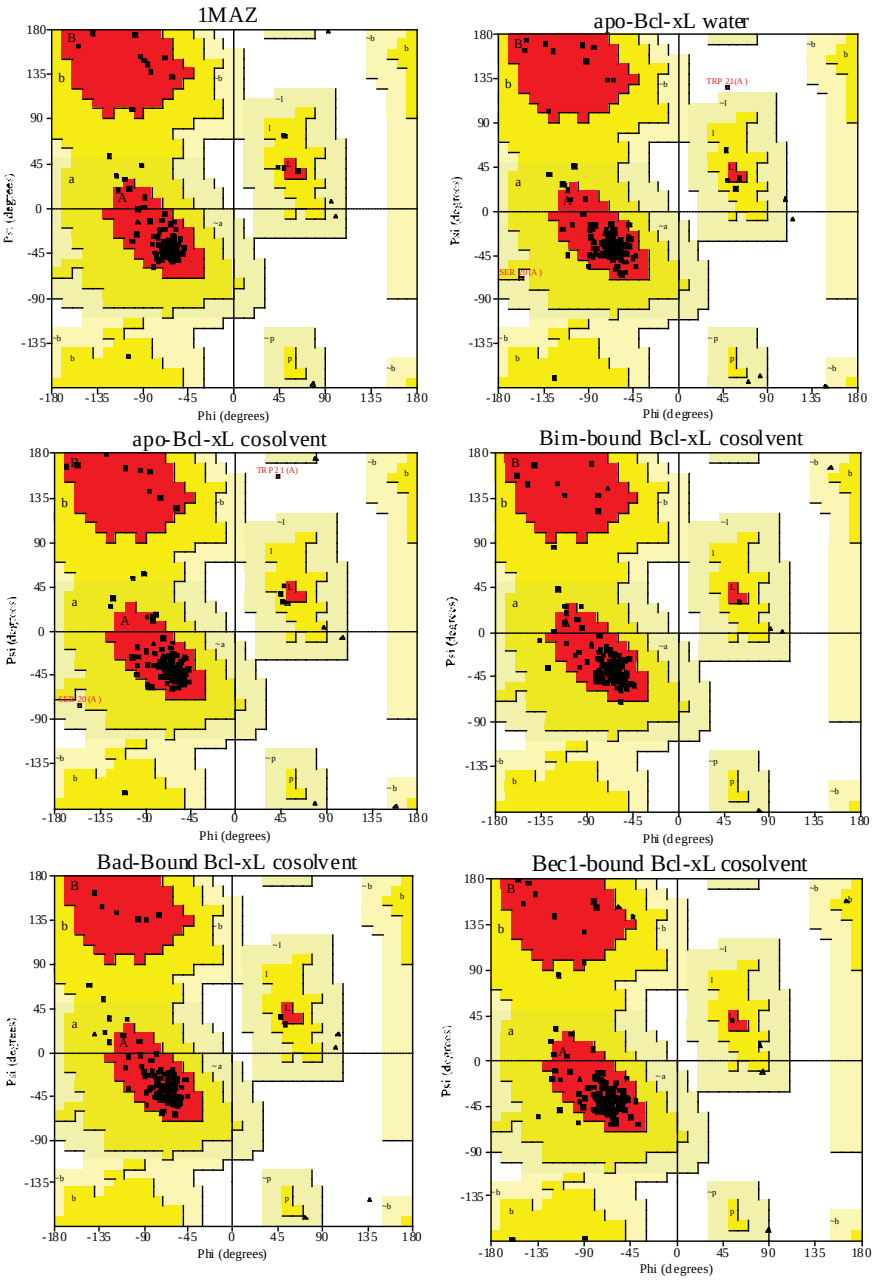

Conformations	1MAZ	apo-Bcl-xL (w)	apo-Bcl-xL (c)	Bim-bound (c)	Bad-bound(c)	Bec1-bound (c)
Residues in most favored regions	94.50%	89.30%	90.20%	93.40%	92.60%	90.20%
Residues in allowed regions	5.50%	9.00%	8.20%	6.60%	7.40%	9.80%
Residues in generous allowed regions		0.80%	0.80%			
Residues in disallowed regions		0.80%	0.80%			

Figure S7. Backbone RMSD of Bim-, Bad-, Bec1-bound Bcl-xL simulated in the water (black line) and the cosolvent (red) environment. The crystal structures of the peptide-bound Bcl-xL were used as the reference structures in each case when calculating backbone RMSD.

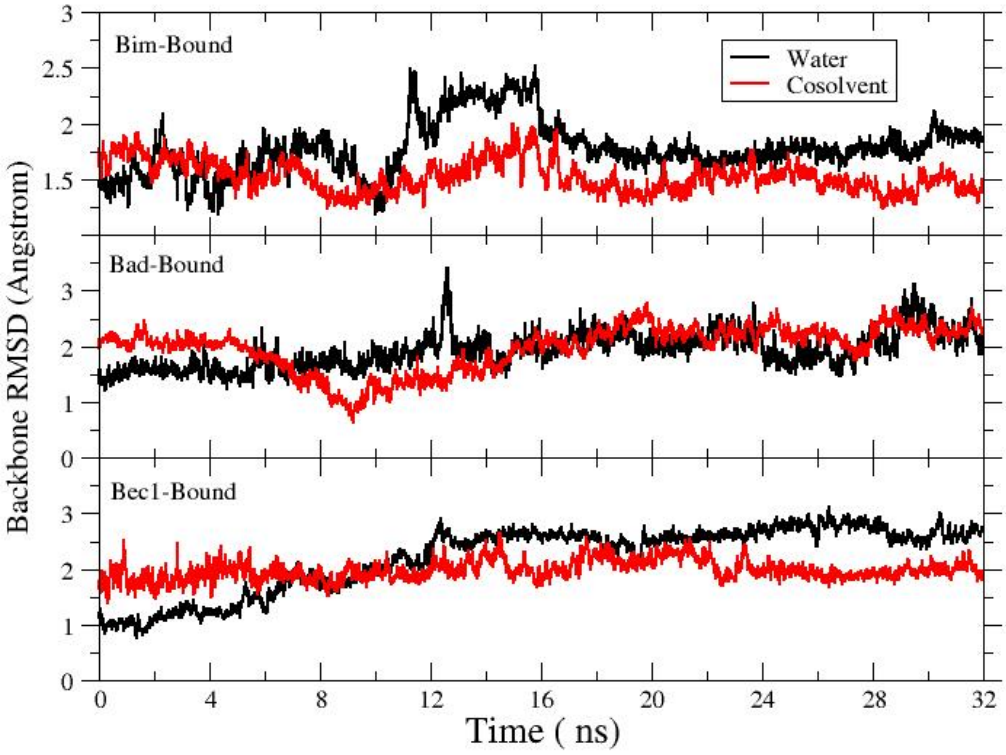

Table S1. Resolutions of the crystal structures used in this work.

PDB ID	Resolution (Å)
1MAZ	2.2
3FDL	1.78
2BZW	2.3
2P1L	2.5
2YXJ	2.2
3INQ	2

References:

(1) Berman, H. M.; Westbrook, J.; Feng, Z.; Gilliland, G.; Bhat, T. N.; Weissig, H.; Shindyalov, I. N.; Bourne, P. E. *Nucl. Acids Res.* **2000**, *28*, 235.

(2) Li, H.; Robertson, A. D.; Jensen, J. H. *Proteins* **2005**, *61*, 704.

(3) Bas, D. C.; Rogers, D. M.; Jensen, J. H. *Proteins* **2008**, *73*, 765.

(4) Case, D. A.; Darden, T. A.; T.E. Cheatham, I.; Simmerling, C. L.; Wang, J.; Duke, R. E.; Luo, R.; Crowley, M.; Walker, R. C.; Zhang, W.; Merz, K. M.; B.Wang; Hayik, S.; Roitberg, A.; Seabra, G.; Kolossváry, I.; K.F.Wong; Paesani, F.; Vanicek, J.; X.Wu; Brozell, S. R.; Steinbrecher, T.; Gohlke, H.; Yang, L.; Tan, C.; Mongan, J.; Hornak, V.; Cui, G.; Mathews, D. H.; Seetin, M. G.; Sagui, C.; Babin, V.; Kollman, P. A.; AMBER10, University of California, San Francisco: 2008.

(5) Wang, J.; Cieplak, P.; Peter A. Kollman *Journal of Computational Chemistry* **2000**, *21*, 1049.

(6) Jorgensen, W. L.; Chandrasekhar, J.; Madura, J. D.; Impey, R. W.; Klein, M. L. *The Journal of Chemical Physics* **1983**, *79*, 926.

(7) Ryckaert, J.-P.; Ciccotti, G.; Berendsen, H. J. C. *Journal of Computational Physics* **1977**, *23*, 327.

(8) Darden, T.; York, D.; Pedersen, L. *Journal of Chemical Physics* **1993**, *98*, 10089.

(9) Laskowski, R. A.; Rullmannn, J. A.; MacArthur, M. W.; Kaptein, R.; Thornton, J. M. *J Biomol NMR* **1996**, *8*, 477.

(10) Laskowski, R. A.; Macarthur, M. W.; Moss, D. S.; Thornton, J. M. *Journal of Applied Crystallography* **1993**, *26*, 283.

(11) Seco, J.; Luque, F. J.; Barril, X. *Journal of Medicinal Chemistry* **2009**, *52*, 2363.

(12) Yang, C.-Y.; Wang, S. *ACS Medicinal Chemistry Letters* **2010**, *1*, 125.